
COMPACT RING RESONATOR ENHANCED SILICON-MSM PHOTODETECTOR IN SiN-ON-SOI PLATFORM

A PREPRINT

Avijit Chatterjee*

Center for Nano Science and Engineering
Indian Institute of Science Bangalore
avijit@iisc.ac.in

Saumitra Sam

Molecular Biophysics Unit
Indian Institute of Science Bangalore

Sujit Kumar Sikdar

Molecular Biophysics Unit
Indian Institute of Science Bangalore

Shankar Kumar Selvaraja

Center for Nano Science and Engineering
Indian Institute of Science Bangalore
shankarks@iisc.ac.in

July 13, 2020

ABSTRACT

We present a compact on-chip resonator enhanced silicon-MSM photodetector in 850 nm wavelength band for communication and lab-on-chip bio-sensing applications. We report the highest responsivity of 0.81 A/W for a 5 μm long device. High responsivity is achieved by integrating the detector in a silicon nitride ring resonator. The resonance offers 100X responsivity improvement over a single-pass photodetector due to cavity enhancement. We also present a detailed study of the high-speed response of the cavity and single-pass detector. We report an electro-optic bandwidth of 7.5 GHz measured using a femtosecond optical excitation. To the best of our knowledge, we report for the first time silicon nitride resonator integrated Si-MSM detector in SiN-SOI platform.

Keywords Integrated optics · Silicon photodetector · Ring resonator enhanced photodetector

1 Introduction

Exponential growth of internet traffic pose the requirement for ultra-high data rate communication links. Integrated optical interconnect is a promising candidate to offer high-speed, scalable, and affordable solution in such situations[1, 2, 3]. In an optical interconnect, one of the key components is a high-speed photodetectors[4, 5, 2, 1, 3, 6]. Silicon photonics based on-chip interconnects with highly efficient Ge/III-V photodetectors is already a very matured, and commercially used platform[7, 8, 9, 10, 11]. For short reach optical interconnects at 850 nm wavelength, silicon photodetector is also explored in addition to Ge and III-V photodetectors[12, 13, 14]. The reason is that the silicon photodetectors have higher responsivity than Ge/III-V at 850 nm wavelength and CMOS compatible fabrication. However, silicon has lower bandwidth than Ge or III-V, which limits its application for high-speed interconnects. To improve the bandwidth of silicon photodetectors, recently thin silicon-on-insulator (SOI) platform is explored [15, 16, 17, 18]. For a conventional top illuminated photodetector, thin silicon reduces the cross-section area and improves the RC time limited bandwidth resulting in sub-picosecond response time [19]. However, reduced cross-section area decreases responsivity [19]. To obtain higher responsivity without degrading bandwidth, waveguide photodetector configuration is a better option than a top illuminated photodetector. An on-chip lateral silicon pin photodetector integrated with SiN waveguide on SiN-SOI platform with higher responsivity (0.44 A/W) and large bandwidth (14 GHz) was demonstrated in [20]. Waveguide integrated photodetector also offers opportunity for on-chip passive optical device integration, such as wavelength selective devices that are essential for next-generation

*Corresponding author: avijit@iisc.ac.in

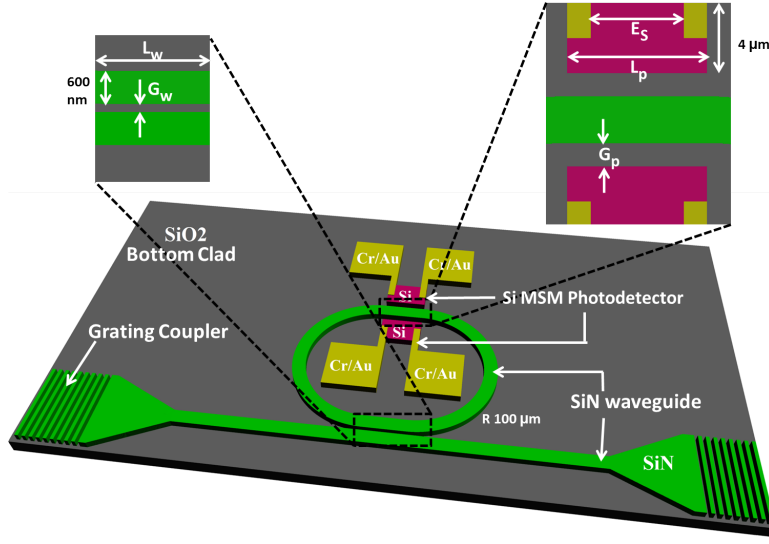


Figure 1: Schematic of a ring coupled silicon-MSM photodetector (RCPD)

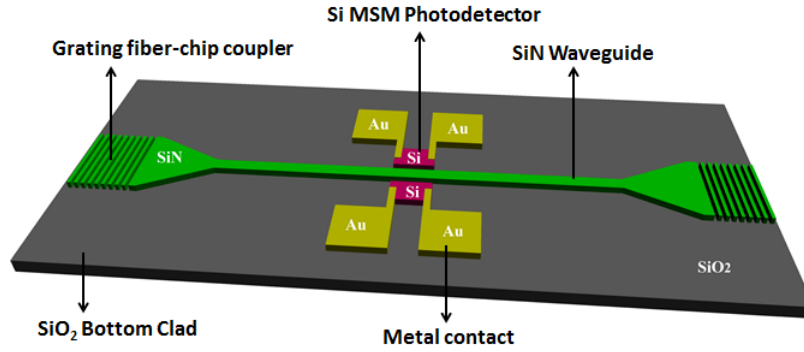


Figure 2: Schematic of a waveguide coupled silicon-MSM photodetector (WGPD)

optical datacom and lab-on-chip bio-sensing application. The responsivity and bandwidth of an integrated silicon photodetector need to improve further, to attain the 400 Gbps road map for short-reach optical datacom [5]. Therefore, the challenge is to increase the responsivity of the photodetector without increasing the physical size to maintain high bandwidth. To achieve high responsivity and bandwidth, one of the solutions is a cavity enhanced photodetector [21, 22, 23, 24, 25, 26, 27, 28]. In the cavity enhanced photodetector, the photodetector is placed inside a resonating cavity. Since the cavity offers optical field enhancement, one could achieve higher responsivity [22, 21, 23, 26]. In addition, the cavity size can be made compact to achieve large bandwidth. In literature various cavity configuration such as Bragg mirror [22], photonic crystal [27, 27], ring resonator[29], and metal reflector [30] were used to realize the cavity enhanced photodetector.

In this paper, we demonstrate silicon nitride (SiN) ring resonator enhanced silicon metal-semiconductor-metal (MSM) photodetector in the 850 nm wavelength band on a SiN-SOI platform. In recent years, SiN has emerged as a versatile platform for integrated photonic circuit for broad spectrum of applications [31, 32, 33]. The emergence is due to broad wavelength transparency and CMOS compatibility. Since SiN is a dielectric material, active functionality such as light modulation, generation and detection requires heterogeneous or monolithic integration of suitable material. In this work, we demonstrate CMOS compatible monolithic integration of Si photodetector. In particular, we demonstrate waveguide Si-MSM photodetector integrated in a SiN ring resonator. Unlike doped junction photodetector, MSM photodetector offers high speed and lower dark current [19]. In addition, MSM fabrication is not as demanding as doped junction. In a doped junction photodetector, the size of the photodetector depends on the control of junction alignment and dopant diffusion control [34]. However, in a MSM detector fabrication, the metal electrodes can be lithographically defined with sub-50 nm alignment accuracy. In this paper, we focus on realizing high-speed and high responsivity waveguide integrated Si photodetector integrated with SiN ring resonator on a single platform for 850 nm based short reach optical interconnects.

2 Design and simulation

Figure 1 shows a schematic of the proposed ring coupled silicon MSM photodetector (RCPD). The proposed device comprises of a race-track SiN ring resonator and Si-MSM photodetector. A Si-MSM photodetector is integrated with the SiN ring resonator in such a way that the circulating optical field inside the SiN ring resonator evanescently couples into the Si photodetector. The gap (G_p) and the interaction length (L_p) between the photodetector and SiN waveguide determine power coupling efficiency and responsivity subsequently. The SiN waveguide circuit was designed to operate in single-mode (TE) regime at 850 nm. Accordingly, based on modal calculations, SiN waveguide width and thickness of 600 nm and 220 nm were chosen, respectively. Light coupling between an optical fiber and the waveguide is achieved using a grating coupler and adiabatic taper [20]. The grating were 220 nm etched with a grating period of 650 nm.

In addition to RCPD, a conventional waveguide integrated Si-MSM photodetector (WGPD) as shown in Fig. 2 is also realized to compare the performance with the RCPD. The configuration and design dimensions of RCPD and WGPD are made identical in order to evaluate the responsivity enhancement of RCPD over WGPD.

A racetrack ring resonator is used as a cavity. The design parameters are optimized using FDTD simulations [35]. The gap between the ring resonator and the bus waveguide (G_w), and the coupling length (L_w) are optimized to achieve required power coupling into the ring. Figure 1 illustrates a racetrack ring resonator with integrated Si-MSM detector. The waveguide width of the ring and bus waveguide are kept identical at 600 nm. A ring radius of 100 μm is chosen to reduce the bend loss. The resonator is operated in a critically coupled regime to achieve sufficient power coupling into the cavity. To achieve critical coupling, the cavity loss is estimated from the propagation loss measurement. A propagation loss of 2.5 dB/mm is obtained from cut-back method. The propagation loss is dominated by the sidewall roughness from the fabrication process. By optimizing the fabrication process, one could achieve one-order lower loss [33]. Based on the estimated cavity round trip loss, required coupling efficiency is obtained by optimizing G_w and L_w [36]. Figure 3 shows the power coupling in a directional coupler and the effect of L_w and G_w between the waveguides on the coupling efficiency. Based on the simulation and fabrication limitations, we used $G_w = 150$ nm and $L_w = 6$ μm as the optimum design parameters.

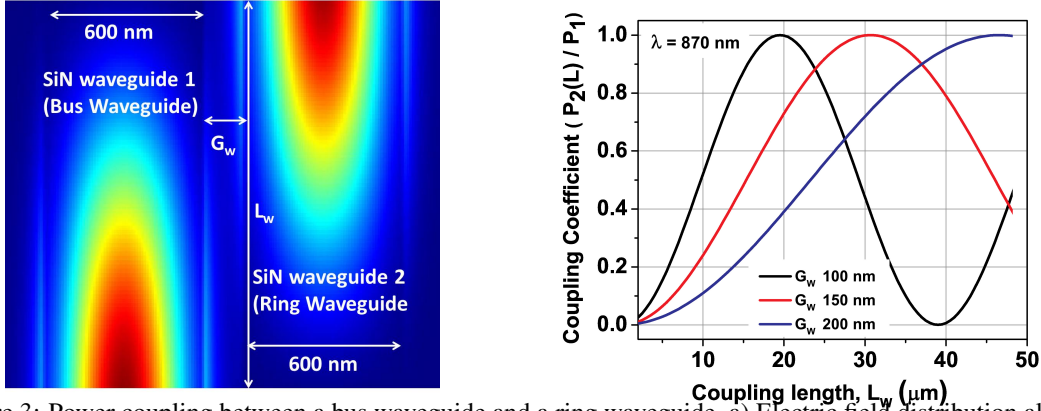


Figure 3: Power coupling between a bus waveguide and a ring waveguide, a) Electric field distribution along the length of the directional coupler and b) coupling efficiency as a function of coupling length (L_w) for varying gap (G_w)

In addition to power coupling into the ring, coupling from SiN ring waveguide into Si photodetector needs to be optimized to achieve optimum responsivity enhancement. It is essential to maintain a circulating optical field in the ring resonator. The power enhancement in the cavity depends on the absorption in the Si-MSM detector and loss in the SiN ring waveguide. An excess optical power loss in the cavity will diminish the circulating power in the resonator resulting in resonance degradation. Since the field enhancement in the cavity is crucial in achieving responsivity enhancement, the power coupling into the cavity and the detector needs careful optimization. Considering the cavity loss, we have chosen G_p as 100 nm and varied L_p in the range of 3-6 μm to study the effect of coupling and cavity loss.

3 Fabrication

The device is fabricated on a SOI wafer with 220 nm thick silicon device layer on a 2 μm thick buried oxide. An overview of the fabrication process flow is illustrated in Fig. 4. After standard wafer clean, Si was patterned using electron-beam lithography (EBL) followed by inductively coupled reactive-ion etching (ICP-RIE) forming islands of Si (Fig. 4b). A 50 nm thick liner SiO_2 followed by 220 nm thick SiN by PECVD and LPCVD, respectively. The liner

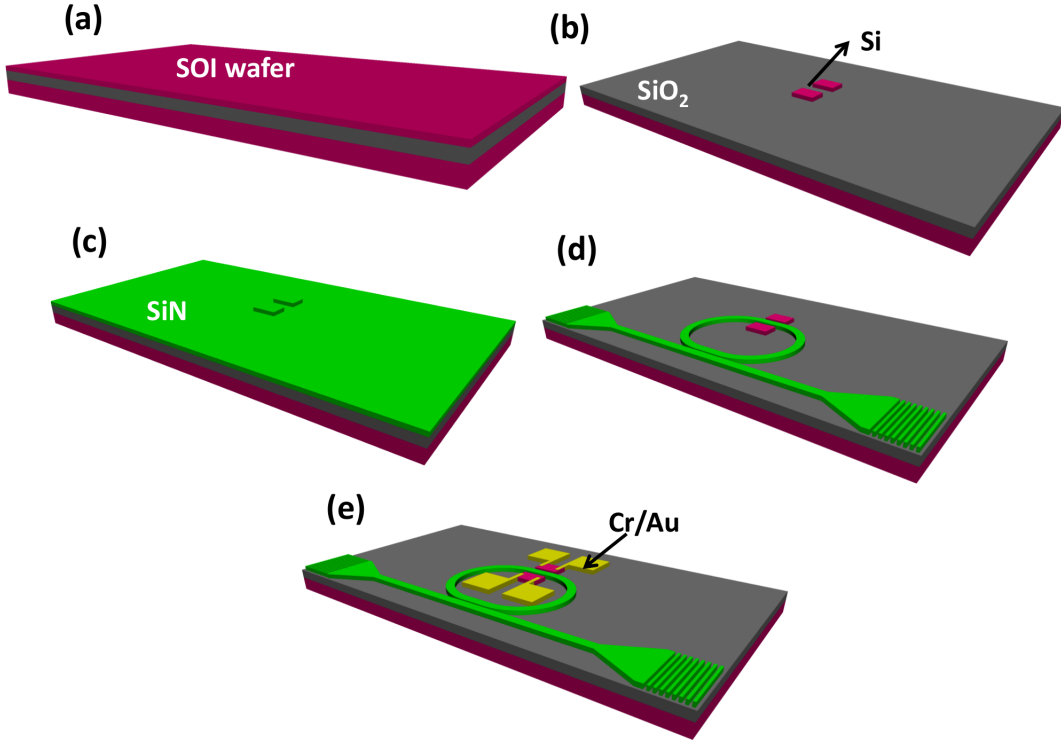


Figure 4: Fabrication process flow overview; (a) Cleaned SOI wafer, (b) silicon patterned by e-beam lithography and dry etching, (c) 50 nm PECVD SiO_2 and 220 nm LPCVD SiN deposited, (d) SiN is patterned by e-beam lithography and dry etching, (e) Chrome/Gold contacts made by e-beam lithography, e-beam evaporation and lift off

oxide acts as a passivation layer, and etch-step layer for SiN. The SiN layer was then patterned using EBL and dry etching of 220 nm thick SiN by ICP-RIE to define the waveguide, the grating coupler, and the ring resonators in a single patterning step. The SiN over the detector region is removed during the etch process stopping on the liner oxide. Finally, chrome-gold electrical contacts were formed on Si using a lift-off process. Figure 5 shows optical and scanning electron microscope image of one of the fabricated cavity Si-MSM photodetector.

4 Results and discussion

The fabricated devices were characterized for static and dynamic optoelectronic characteristics. The static characteristics were measured using source measurement units while the dynamic response was measured using a pulsed laser and a high-speed oscilloscope.

4.1 I-V characteristic of ring resonator enhanced silicon-MSM photodetector

Electrical response was measured for Si-MSM photodetector under dark and light condition. An LED source with the wavelength range of 860-900 nm was used for the measurement. Light from an LED source is coupled using an optical fiber into the waveguide through grating coupler. The spectral response of resonator was captured by an optical spectrum analyzer (OSA). To bias the Si-MSM photodetector and measure the output current, source measuring unit (Keithley 2401) and DC probes were used.

Figure 6 shows the normalized transmission response of the fabricated ring resonator with and without Si-MSM photodetector. The obtained spectrum is normalized with a reference waveguide. A coupling efficiency of 14 dB/coupler at 860 nm and a 1-dB bandwidth of 12 nm was measured from the reference waveguide. The spectral response of the ring with and without MSM photodetector clearly shows the effect of Si-MSM. We observe an increase of ≈ 4 dB in insertion and ≈ 8 dB in extinction due to Si-MSM in the ring cavity (Fig. 7). In addition, a marginal increase in the

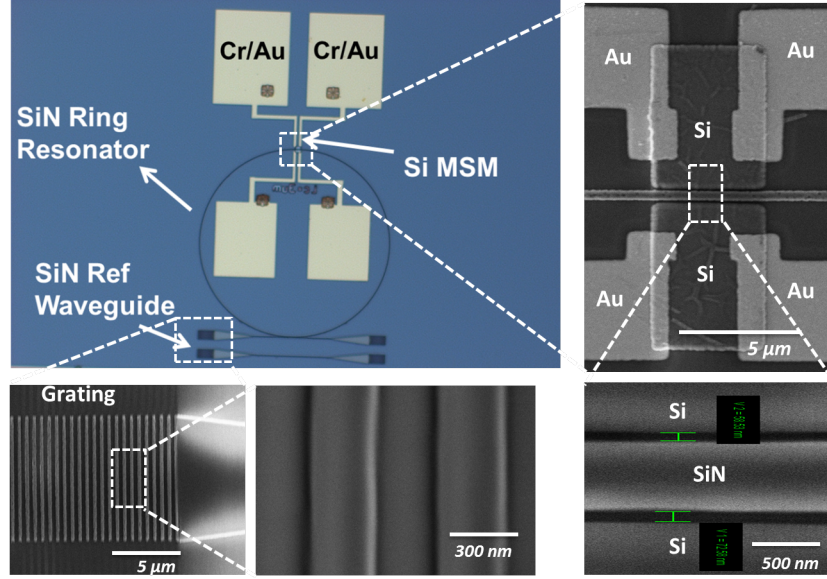


Figure 5: Optical and scanning electron microscope image of a fabricated ring coupled Si-MSM detector.

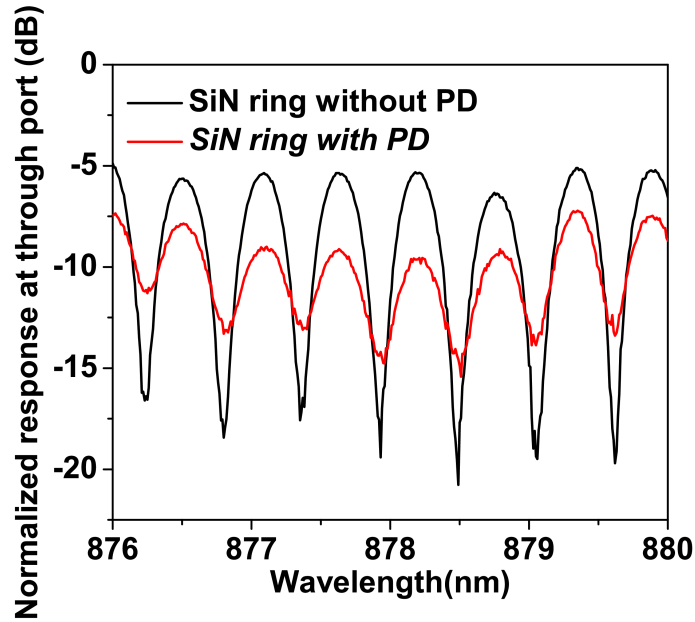


Figure 6: Normalized through port ring resonator spectral response; with and without Si-MSM integration.

quality factor due to the detector (Fig. 7b). The increase in the quality factor can be attributed to ring response moving towards critical coupling from an over-coupled regime.

Figure 8 (a) summarizes I-V characteristics of the Si-MSM photodetector with and without optical excitation. Figure 8 (a) and (b) also shows a comparison between the ring coupled detector (RCPD) and waveguide coupled detector (WGPD). The RCPD shows lower dark current of ≈ 0.8 nA compared to 10 nA measured at -5 V bias for a WGPD of same detector dimension. Though the length of the detector is the same for WGPD and RCPD, RCPD measures lower dark current. This is due to a minor difference in the contact configuration between the two detector configuration. In RCPD, the electrodes on the outer and inner side of the ring have different spacing which substantially reduces the dark current, while in a WGPD the electrodes are equally placed on both sides of the waveguide. Furthermore, the asymmetry in the IV characteristics is due to asymmetric contacts. We measure a photocurrent of $1 \mu\text{A}$ for an RCPD

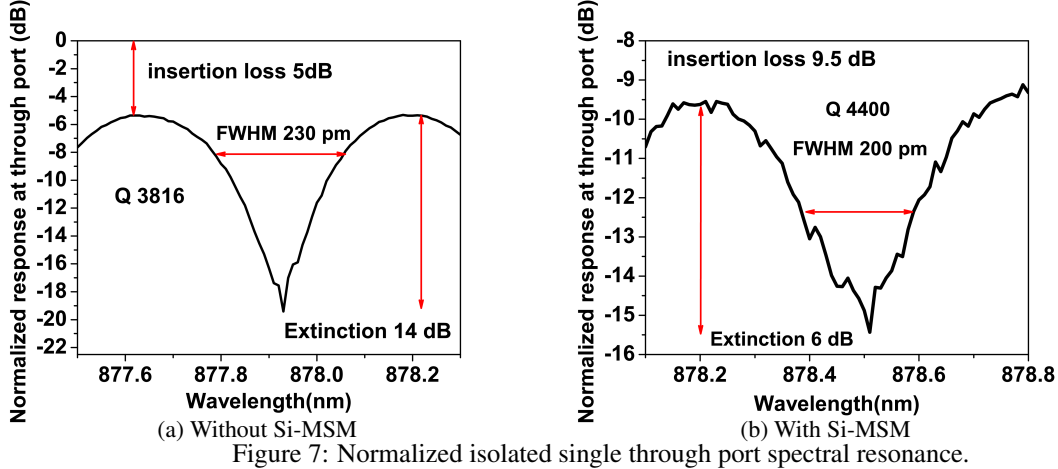


Figure 7: Normalized isolated single through port spectral resonance.

Table 1: Performance comparison between waveguide coupled photodetector (WGPD) and ring coupled photodetector (RCPD) for different coupling gap G_w , coupling length L_w , and detector length L_p as depicted in Fig. 1 and Fig. 2.

Parameters	Bias (V)	WGPD $L_p = 6 \mu m$	RCPD			
			$G_w = 150 \text{ nm}$		$G_w = 200 \text{ nm}$	
			$L_w = 5 \mu m$ $L_p = 5 \mu m$	$L_w = 6 \mu m$ $L_p = 6 \mu m$	$L_w = 5 \mu m$ $L_p = 5 \mu m$	$L_w = 6 \mu m$ $L_p = 6 \mu m$
Dark Current (nA)	1	3.76	3.00	3.76	0.99	1.12
	3	6.39	9.28	6.39	1.41	5.23
	5	7.45	13.1	7.45	1.81	7.20
Photocurrent (nA)	1	49.9	452	762	486	472
	3	59.2	566	792	571	515
	5	66.6	587	797	596	545
Responsivity (A/W)	1	0.005	0.6	0.76	0.16	0.69
	3	0.006	0.76	0.79	0.19	0.75
	5	0.007	0.78	0.80	0.2	0.80

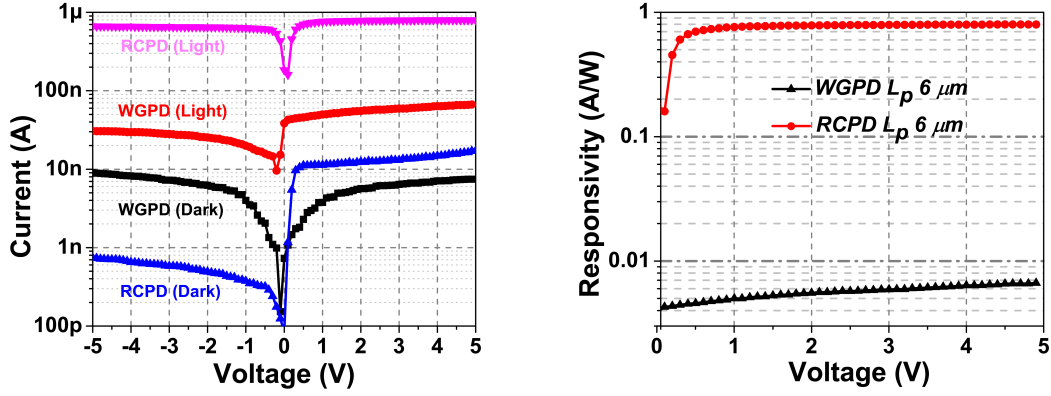
and 30 nA for a WGPD with a bias of -5 V. Unlike WGPD, due to cavity enhancement RCPD shows three orders of magnitude increase in light current under illumination.

4.2 Responsivity estimation

The responsivity of the RCPD is estimated from the optical power in the ring waveguide. First, power coupled into the bus waveguide is calculated by deducting the fiber to grating coupler loss. The power coupled from the waveguide into the ring is estimated from the directional coupler (Fig. 3). Further, the enhancement due to the cavity is also considered in responsivity calculation.

The responsivity of the RCPD and WGPD is calculated from the power coupling, and IV characterizes. We measure a responsivity of 0.79 A/W at 5 V for an RCPD, which is two orders higher than the WGPD (Fig. 8b). Improvement in responsivity is attributed to the enhanced optical field inside the ring and absorption of optical power [26, 25]. We observe a marginal increase in the responsivity due to higher field between the electrodes that efficiently sweeps the photo-generated carriers.

The quality factor of the ring resonator has a direct influence on the detector responsivity. Figure 9 shows the effect of light-coupling into the ring and the quality factor. For the devices with quality factor >3000 , we observe higher responsivity (≈ 0.75 A/W), however, for a device with lower coupling due to larger gap $G_w = 200$ nm and shorter coupling length $L_w = 5 \mu m$ (Fig. 3), we observe a lower responsivity of 0.2 A/W. Cavity enhancement is achieved with optimal coupling between the waveguide and ring that compensates loss in the cavity to achieve decent quality factor. Table 1 summarizes the performance metrics of WGPD and RCPD with various power coupling. With increasing bias, we observe enhanced responsivity due to efficient charge collection; however, with a marginal increase in dark current. Furthermore, as mentioned earlier, the responsivity is low for cavities with lower quality factor.



(a) Current Vs Voltage (b) Responsivity Vs Voltage
Figure 8: IV characteristics and responsivity of waveguide coupled (WGPD) and ring coupled (RCPD) Si-MSM photodetector with $L_p = 6 \mu m$, $G_w = 150 \text{ nm}$, $L_w = 6 \mu m$

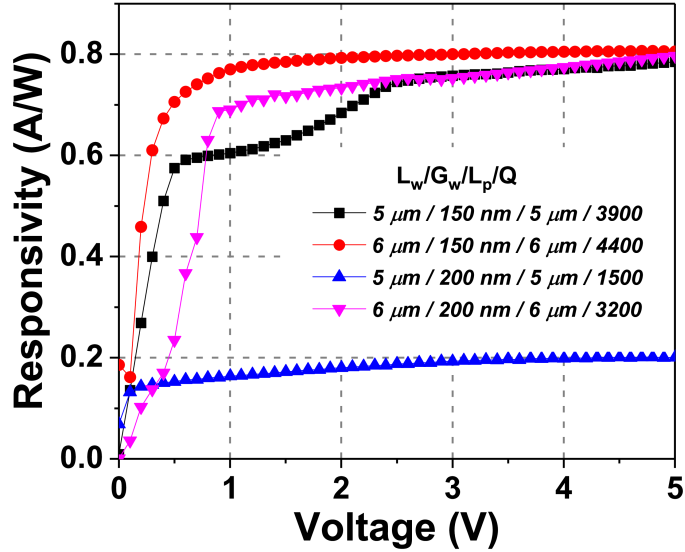


Figure 9: Effect of detector length (L_p), ring coupling ($G_w L_w$), and Q-factor (Q) on the RCPD responsivity at various bias voltages.

4.3 High-frequency response

The frequency response of the Si-MSM photodetector was determined by the impulse response to a femtosecond optical pulse. Light from an 850 nm femtosecond pulsed laser source is coupled through the grating coupler. The full width at half maximum (FWHM) of 280 fs at 80 MHz repetition rate was used for the characterization. The light output from the pulsed laser source was focused vertically on top of the grating. The response of the photodetector was measured through a high-speed RF probe and sampling oscilloscope. A detailed schematic is presented in [20].

Fig 10 (a) and (b) show the temporal response of the ring enhanced Si-MSM photodetector for different ring resonator parameters. The FWHM of the pulse response is used to determine the 3dB bandwidth of the detector as given in Eq. 1 [7].

$$f_{3dB} = \frac{0.45}{FWHM} \quad (1)$$

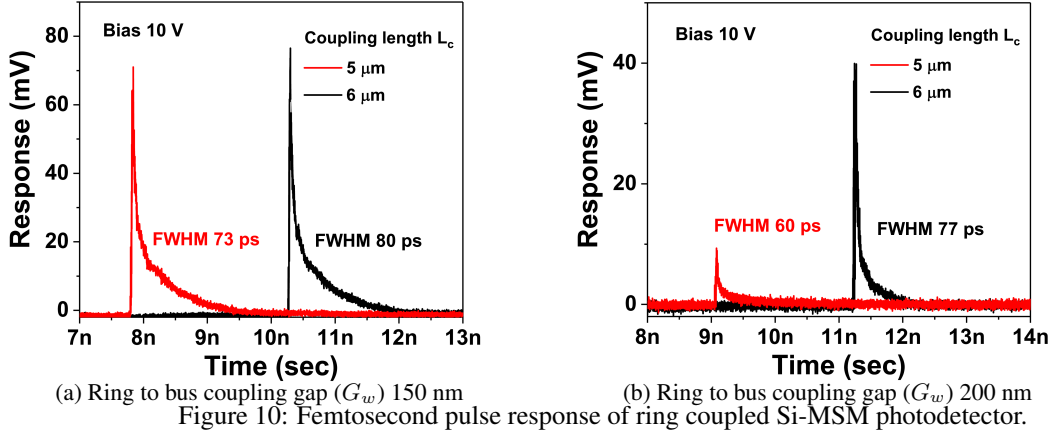


Figure 10: Femtosecond pulse response of ring coupled Si-MSM photodetector.

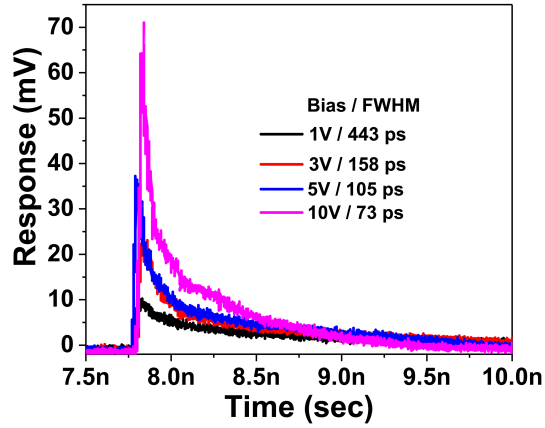


Figure 11: Effect of bias voltage on the pulse response of RCPD ($L_p = 5 \mu\text{m}$, $G_w = 150 \text{ nm}$, and $L_w = 5 \mu\text{m}$)

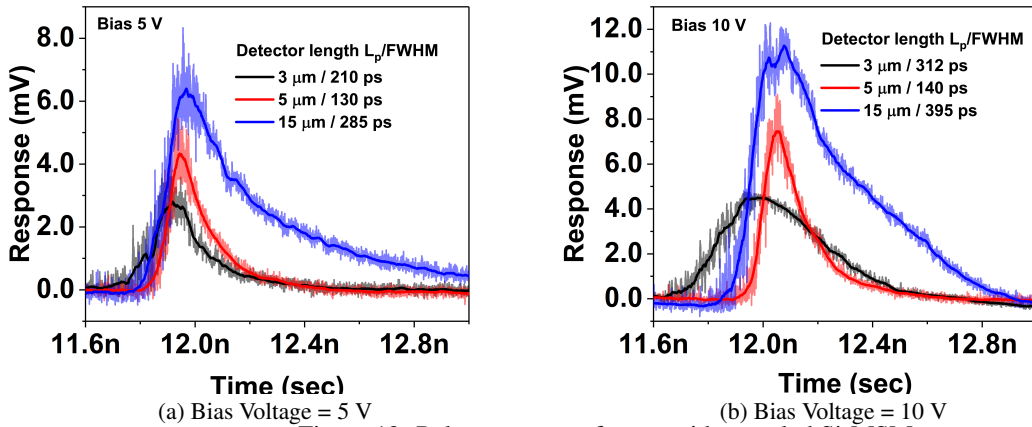


Figure 12: Pulse response of waveguide coupled Si-MSM.

Figure 12 depicts the pulse response of WGPD of various lengths at a bias of 5 V and 10 V. We measure best FWHM of 130 ps corresponds to a f_{3dB} of $3.46 \pm 0.4 \text{ GHz}$ for a detector length of 5 μm . It is evident from Figure 12a and Figure 12b that increasing the bias improves the responsivity; however, the pulse response time increases. Even for the same detector length of 5 μm , at 5 V bias, we measure a pulse response time of 130 ps and 105 ps from WGPD and RCPD,

Table 2: Comparison with various demonstration of photodetectors in 850 nm wavelength band

Ref.	Bias (V)	Dark current (pA/ μm^2)	R (mA/W)	f_{3dB} (GHz)	η (mA/W * GHz)	Platform (Active layer thickness)	Electrode separation	Integrated	Resonant cavity enhancement factor
[19]	1	0.2	5.7	140	798	SOI, Si MSM (100 nm)	100 nm	No	Nil
[37]	9	7.66×10^{-3}	330	Nil	Nil	Poly Si pin (150 nm)	NA	Yes	Nil
[16]	14	2.6×10^3	300	16.4	4920	SOI, Si pin (220 nm)	NA	No	Nil
[15]	5	4×10^{-2}	340	15	5100	Micro structured Si pin (2 μm)	NA	No	Nil
[23]	4	4×10^{-3}	230	0.96	221	SOI, Si pin (2.18 μm)	NA	No	4.6X
[22]	5	2.7×10^{-3}	210	34	7140	Si pin (500 nm)	NA	No	Nil
This work	5	45	790	5	3950	SiN-on-SOI, Si MSM (220 nm)	4 μm	Yes	100X
This work	10	292	810	7.5	6075	SiN-on-SOI, Si MSM (220 nm)	4 μm	Yes	100X

respectively. We attribute the lower bandwidth of WGPD to charge screening effect due to photocurrent saturation [38]. One could decrease the screening effect by reducing the power in the waveguide. However, lower input power would result in lower photocurrent due to poor responsivity of WGPD. Although increasing the length of the photodetector to 15 μm improves the responsivity, the pulse response does not improve. The speed of longer detector is limited by transit time. Thus a trade-off between screening and transit time limit is enviable. A 5 μm long WGPD shows such optimum where we observe response times are better than 3 μm long device with higher responsivity.

Table 2 summarizes reported photodetector performance metrics in the literature. The ring coupled photodetector demonstrated has the highest responsivity-gain product (η). Although silicon pin photodetectors show higher η , MSM based detectors are still attractive due to potential higher bandwidth.

5 Conclusion

In summary, we have demonstrated SiN ring resonator enhanced silicon-MSM photodetector in the 850 nm wavelength band on SiN-SOI platform. Compared to waveguide photodetector, ring enhanced MSM with identical dimension gives two-orders enhancement in responsivity. Responsivity enhancement is attributed to the enhanced optical field inside the ring cavity and absorption of the optical field in the Si-MSM photodetector. As a result of field enhancement, we achieve compact photodetector with high responsivity. We demonstrate a responsivity of 0.81 A/W at 10 V with a 5 μm long detector. The smaller physical size of the photodetector also ensures low RC time constant and hence large bandwidth. With a 5 μm long device, we achieved an electro-optic bandwidth of 7.5 GHz. We also presented a detailed discussion on the effect of device configuration on the photodetector response. In conclusion, on-chip wavelength-selective Si-MSM paves the way to realize a highly efficient, compact, and cost-effective solution for the application in optical interconnects and lab-on-chip bio-sensors in <1100 nm wavelength range.

6 Acknowledgement

We acknowledge funding support from MHRD through NIEIN project, from MeitY and DST through NNetRA project.

References

- [1] David A.B. Miller. Device requirements for optical interconnects to silicon chips. *Proceedings of the IEEE*, 97(7):1166–1185, 2009.
- [2] Marc A. Taubenblatt. Optical interconnects for high-performance computing. *Journal of Lightwave Technology*, 30(4):448–458, 2012.
- [3] Jim A. Tatum, Deepa Gazula, Luke A. Graham, James K. Guenter, Ralph H. Johnson, Jonathan King, Chris Kocot, Gary D. Landry, Ilya Lyubomirsky, Andrew N. MacInnes, Edward M. Shaw, Kasyapa Balemarthy, Roman Shubochkin, Durgesh Vaidya, Man Yan, and Frederick Tang. VCSEL-based interconnects for current and future data centers. *Journal of Lightwave Technology*, 33(4):727–732, feb 2015.
- [4] Richard Soref. The past, present, and future of silicon photonics. *IEEE Journal of selected topics in quantum electronics*, 12(6):1678–1687, 2006.
- [5] IEEE. IEEE p802.bs 400 GbE baseline summary, 2015.
- [6] Christoforos Kachris and Ioannis Tomkos. A Survey on Optical Interconnects for Data Centers. *IEEE Communications Surveys & Tutorials*, 14(4):1021–1036, 2012.
- [7] Long Chen and Michal Lipson. Ultra-low capacitance and high speed germanium photodetectors on silicon. *Opt. Express*, 17(10):7901–7906, May 2009.

- [8] Laurent Vivien, Andreas Polzer, Delphine Marris-Morini, Johann Osmond, Jean Michel Hartmann, Paul Crozat, Eric Cassan, Christophe Kopp, Horst Zimmermann, and Jean Marc Fédéli. Zero-bias 40gbit/s germanium waveguide photodetector on silicon. *Optics express*, 20(2):1096–1101, 2012.
- [9] Zhen Sheng, Liu Liu, Joost Brouckaert, Sailing He, and Dries Van Thourhout. InGaAs PIN photodetectors integrated on silicon-on-insulator waveguides. *Optics express*, 18(2):1756–1761, 2010.
- [10] Liu Liu, Günther Roelkens, Joris Van Campenhout, Joost Brouckaert, Dries Van Thourhout, and Roel Baets. III–V/silicon-on-insulator nanophotonic cavities for optical network-on-chip. *Journal of nanoscience and nanotechnology*, 10(3):1461–1472, 2010.
- [11] Thijs Spuesens, Fabien Mandorlo, Pedro Rojo-Romeo, Philippe Régreny, Nicolas Olivier, Jean-Marc Fedeli, and Dries Van Thourhout. Compact integration of optical sources and detectors on SOI for optical interconnects fabricated in a 200 mm cmos pilot line. *Journal of Lightwave Technology*, 30(11):1764–1770, 2012.
- [12] Guanyu Chen, Jeroen Goyvaerts, Sulakshna Kumari, Joris Van Kerrebrouck, Muhammad Muneeb, Sarah Uvin, Yu Yu, and Gunther Roelkens. Integration of high-speed GaAs metal-semiconductor-metal photodetectors by means of transfer printing for 850 nm wavelength photonic interposers. *Optics express*, 26(5):6351–6359, 2018.
- [13] Berkehan Ciftcioglu, Jie Zhang, Roman Sobolewski, and Hui Wu. An 850-nm normal-incidence germanium metal–semiconductor–metal photodetector with 13-GHz bandwidth and 8- μ A dark current. *IEEE Photonics Technology Letters*, 22(24):1850–1852, 2010.
- [14] B-C Hsu, ST Chang, T-C Chen, P-S Kuo, PS Chen, Z Pei, and CW Liu. A high efficient 820 nm mos Ge quantum dot photodetector. *IEEE Electron Device Letters*, 24(5):318–320, 2003.
- [15] Yang Gao, Hilal Cansizoglu, Kazim G Polat, Soroush Ghandiparsi, Ahmet Kaya, Hasina H Mamtaz, Ahmed S Mayet, Yanan Wang, Xinzhi Zhang, Toshishige Yamada, et al. Photon-trapping microstructures enable high-speed high-efficiency silicon photodiodes. *Nature Photonics*, 11(5):301, 2017.
- [16] Monireh Moayedi Pour Fard, Christopher Williams, Glenn Cowan, and Odile Liboiron-Ladouceur. High-speed grating-assisted all-silicon photodetectors for 850 nm applications. *Optics Express*, 25(5):5107, mar 2017.
- [17] Gen Li, Kazuaki Maekita, Hiroya Mitsuno, Takeo Maruyama, and Koichi Iiyama. Over 10 GHz lateral silicon photodetector fabricated on silicon-on-insulator substrate by CMOS-compatible process. *Japanese Journal of Applied Physics*, 54(4S):04DG06, apr 2015.
- [18] Myung-Jae Lee. First CMOS silicon avalanche photodetectors with over 10-GHz bandwidth. *IEEE Photonic Tech L*, 28(3):276–279, feb 2016.
- [19] MY Liu, E Chen, and Stephen Y Chou. 140-GHz metal-semiconductor-metal photodetectors on silicon-on-insulator substrate with a scaled active layer. *Applied physics letters*, 65(7):887–888, 1994.
- [20] Avijit Chatterjee, Sujit Kumar Sikdar, Shankar Kumar Selvaraja, et al. High-speed waveguide integrated silicon photodetector on a SiN-SOI platform for short reach datacom. *Optics letters*, 44(7):1682–1685, 2019.
- [21] Gerold W Neudeck, Jack Denton, J Qi, JD Schaub, R Li, and JC Campbell. Selective epitaxial growth si resonant-cavity photodetector. *IEEE Photonics Technology Letters*, 10(1):129–131, 1998.
- [22] JD Schaub, R Li, CL Schow, JC Campbell, GW Neudeck, and J Denton. Resonant-cavity-enhanced high-speed Si photodiode grown by epitaxial lateral overgrowth. *IEEE Photonics Technology Letters*, 11(12):1647–1649, 1999.
- [23] BW Cheng, CB Li, Fei Yao, CL Xue, JG Zhang, RW Mao, YH Zuo, LP Luo, and QM Wang. Silicon membrane resonant-cavity-enhanced photodetector. *Applied Physics Letters*, 87(6):061111, 2005.
- [24] Luca Alloatti and Rajeev Jagga Ram. Resonance-enhanced waveguide-coupled silicon-germanium detector. *Applied Physics Letters*, 108(7):071105, 2016.
- [25] Maurizio Casalino. Design of resonant cavity-enhanced schottky Graphene/silicon photodetectors at 1550 nm. *Journal of Lightwave Technology*, 36(9):1766–1774, 2018.
- [26] Bo-Jun Huang, Jun-Han Lin, H. H. Cheng, and Guo-En Chang. GeSn resonant-cavity-enhanced photodetectors on silicon-on-insulator platforms. *Opt. Lett.*, 43(6):1215–1218, Mar 2018.
- [27] Kengo Nozaki, Shinji Matsuo, Takuro Fujii, Koji Takeda, Masaaki Ono, Abdul Shakoore, Eiichi Kuramochi, and Masaya Notomi. Photonic-crystal nano-photodetector with ultrasmall capacitance for on-chip light-to-voltage conversion without an amplifier. *Optica*, 3(5):483–492, 2016.
- [28] Hao Zhou, Tingyi Gu, James F McMillan, Mingbin Yu, Guoqiang Lo, Dim-Lee Kwong, Guoying Feng, Shouhuan Zhou, and Chee Wei Wong. Enhanced photoresponsivity in graphene-silicon slow-light photonic crystal waveguides. *Applied Physics Letters*, 108(11):111106, 2016.

- [29] Junfeng Song, Andy Lim Eu-Jin, Xianshu Luo, Ying Huang, Xiaoguang Tu, Lianxi Jia, Qing Fang, Tsung-Yang Liow, Mingbin Yu, and Guo-Qiang Lo. A microring resonator photodetector for enhancement in l-band performance. *Optics express*, 22(22):26976–26984, 2014.
- [30] Stephane Collin, Fabrice Pardo, and Jean-Luc Pelouard. Resonant-cavity-enhanced subwavelength metal–semiconductor–metal photodetector. *Applied physics letters*, 83(8):1521–1523, 2003.
- [31] AZ Subramanian, Pieter Neutens, Ashim Dhakal, Roelof Jansen, Tom Claes, Xavier Rottenberg, Frédéric Peyskens, Shankar Selvaraja, Philippe Helin, Bert Du Bois, et al. Low-loss singlemode PECVD silicon nitride photonic wire waveguides for 532-900 nm wavelength window fabricated within a cmos pilot line. *IEEE Photonics Journal*, 5(6):2202809–2202809, 2013.
- [32] Guanyu Chen, Jeroen Goyvaerts, Sulakshna Kumari, Joris Van Kerrebrouck, Muhammad Muneeb, Sarah Uvin, Yu Yu, and Gunther Roelkens. Integration of high-speed GaAs metal-semiconductor-metal photodetectors by means of transfer printing for 850 nm wavelength photonic interposers. *Opt. Express*, 26(5):6351–6359, Mar 2018.
- [33] Nicola Daldosso, Mirko Melchiorri, Francesco Riboli, Manuel Girardini, Georg Pucker, Michele Crivellari, Pierluigi Bellutti, Alberto Lui, and Lorenzo Pavesi. Comparison among various SiN waveguide geometries grown within a CMOS fabrication pilot line. *Journal of Lightwave Technology*, 22(7):1734–1740, 2004.
- [34] Vadivukkarasi Jeyaselvan and Shankar Kumar Selvaraja. Lateral dopant diffusion length measurements using silicon microring resonators. *IEEE Photonics Technology Letters*, 30(24):2163–2166, 2018.
- [35] FDTD Lumerical. Solutions, 2016.
- [36] Mode Solutions. version 4.0, lumerical solutions. Inc. Available: <http://www.lumerical.com>.
- [37] Alina Samusenko, Davide Gandolfi, Georg Pucker, Tatevik Chalyan, Romain Guider, Mher Ghulinyan, and Lorenzo Pavesi. A SiON microring resonator-based platform for biosensing at 850 nm. *Journal of Lightwave Technology*, 34(3):969–977, 2016.
- [38] LY Lin, MC Wu, T Itoh, TA Vang, RE Muller, DL Sivco, and AY Cho. High-power high-speed photodetectors-design, analysis, and experimental demonstration. *IEEE Transactions on Microwave Theory and Techniques*, 45(8):1320–1331, 1997.